LIMNOLOGY and OCEANOGRAPHY

ASLO

Limnol. Oceanogr. 69, 2024, 2211–2228

doi: 10.1002/lno.12666

Divergent metabolism estimates from dissolved oxygen and inorganic carbon: Implications for river carbon cycling

Qipei Shangguan,[1] **Robert A. Payn**,[2,3] **Robert O. Hall Jr**,[4] **Fischer L. Young**,[1] **H. Maurice Valett**,[5] **Michael D. DeGrandpre**[1*]

[1]Department of Chemistry and Biochemistry, University of Montana, Missoula, Montana, USA
[2]Department of Land Resources and Environmental Sciences, Montana State University, Bozeman, Montana, USA
[3]Montana Institute on Ecosystems, Montana University System, Bozeman, Montana, USA
[4]Flathead Lake Biological Station, University of Montana, Polson, Montana, USA
[5]Division of Biological Sciences, University of Montana, Missoula, Montana, USA

Abstract

Rivers efficiently collect, process, and transport terrestrial-derived carbon. River ecosystem metabolism is the primary mechanism for processing carbon. Diel cycles of dissolved oxygen (DO) have been used for decades to infer river ecosystem metabolic rates, which are routinely used to predict metabolism of carbon dioxide (CO_2) with uncertainties of the assumed stoichiometry ranging by a factor of 4. Dissolved inorganic carbon (DIC) has been less used to directly infer metabolism because it is more difficult to quantify, involves the complexity of inorganic carbon speciation, and as shown in this study, likely requires a two-station approach. Here, we developed DIC metabolism models using single- and two-station approaches. We compared metabolism estimates based on simultaneous DO and DIC monitoring in the Upper Clark Fork River (USA), which also allowed us to estimate ecosystem-level photosynthetic and respiratory quotients (PQ_E and RQ_E). We observed that metabolism estimates from DIC varied more between single- and two-station approaches than estimates from DO. Due to carbonate buffering, CO_2 is slower to equilibrate with the atmosphere compared to DO, likely incorporating a longer distance of upstream heterogeneity. Reach-averaged PQ_E ranged from 1.5 to 2.0, while RQ_E ranged from 0.8 to 1.5. Gross primary production from DO was larger than that from DIC, as was net ecosystem production by 100 mmol m^{-2} d^{-1}. The river was autotrophic based on DO but heterotrophic based on DIC, complicating our understanding of how metabolism regulated CO_2 production. We suggest future studies simultaneously model metabolism from DO and DIC to understand carbon processing in rivers.

The transport and processing of dissolved inorganic carbon (DIC) in rivers and streams are considerably an important parts of the global carbon cycle. DIC comprises dissolved CO_2, bicarbonate (HCO_3^-) ions, and carbonate ions (CO_3^{2-}) that are in chemical equilibrium in water (Fig. 1). Dissolved CO_2 is the gaseous form that exchanges with the atmosphere and is thus often quantified as the partial pressure of CO_2 (pCO_2) to allow direct comparisons with atmospheric equilibration. Rivers and streams (hereafter, rivers) provide a pathway for efficient export of DIC through atmospheric CO_2 emissions (Butman and Raymond 2011; Raymond et al. 2013; Lauerwald et al. 2015) and downstream flow to the coastal oceans. Riverine DIC originates mostly from DIC in groundwater inflows and aquatic ecosystem respiration of terrestrially derived organic matter (Cole et al. 2007; Butman et al. 2016; Drake et al. 2018). The relative contributions of these processes greatly vary between and within rivers (Hotchkiss et al. 2015), and our ability to model and predict DIC fluxes remains limited (Battin et al. 2023).

Gross primary production (GPP) and ecosystem respiration (ER) in river ecosystems have a strong influence on DIC dynamics, but these processes are usually estimated from diel cycles of dissolved oxygen (DO) concentrations (i.e., Odum 1956; Demars et al. 2015). The widespread use of

*Correspondence: michael.degrandpre@umontana.edu

Additional Supporting Information may be found in the online version of this article.

Author Contribution Statement: QS analyzed data and wrote the original draft. RAP coded the new models. ROH and RAP refined ideas and assisted QS with modeling. MDD, ROH, and RAP assisted QS with manuscript preparations. MDD conceptualized the study design and undertook the supervision. MDD and HMV coordinated field work. QS and FLY collected the majority of data. HMV, MDD, RAP, and ROH acquired the funding; all authors edited the manuscript.

O_2 is primarily due to early advances in DO sensors (Langdon 1984) and the availability of modeling methods to estimate metabolism from DO data (i.e., Grace et al. 2015; Payn et al. 2017; Appling et al. 2018). Connecting DO metabolism and DIC cycling relies on converting fluxes of DO to DIC by characterizing the whole-ecosystem metabolic photosynthetic quotient (PQ_E) (Trentman et al. 2023) and respiration quotient (RQ_E) (Berggren et al. 2012) (Fig. 1). We differentiate PQ_E from the biochemical photosynthetic quotient (PQ), and RQ_E from the biochemical respiration quotient (RQ) to acknowledge the additional physical and biological ecosystem processes that may greatly alter observed stoichiometric behavior from their cellular-level biochemical controls. Current efforts mostly use fixed values of PQ_E and RQ_E that are based on biochemical assumptions or generalizations of PQ and RQ (Trentman et al. 2023). PQ_E and RQ_E were assumed to be 1 in Rocher-Ros et al. (2020) and the Redfield ratio of 138:106 in Gómez-Gener et al. (2016).

Many ecosystem processes can decouple fundamental biochemical stoichiometric links between DO and DIC, causing the disparities between PQ_E and PQ, or RQ_E and RQ. For example, bubbling of DO from the sediments (ebullition) can contribute up to 20% of DO loss (Howard et al. 2018) without an equivalent loss of CO_2 because DO is less soluble in water than CO_2 and more likely to form bubbles. Similarly, nitrification can consume DO with a much smaller relative change in CO_2 (Pathak et al. 2022). In contrast, calcite precipitation releases CO_2 (Stets et al. 2009) without change in DO. DO models for inferring GPP and ER cannot distinguish each process that contributes to the differential variability of DO and

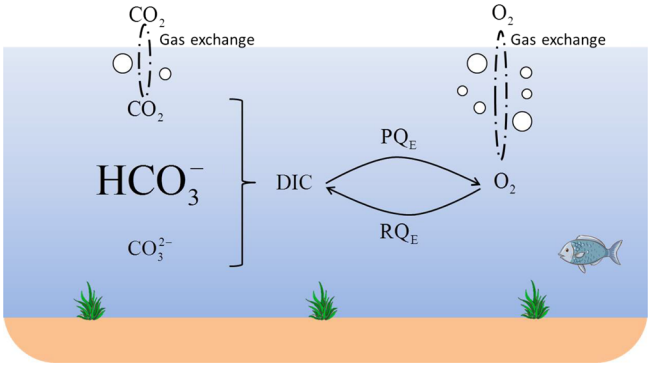

Fig. 1. A conceptual diagram showing biogeochemical cycling of CO_2 and DO (O_2) in alkaline rivers. CO_2 is one of the components in the total DIC pool, while HCO_3^- accounts for the majority under most conditions. Due to the DIC speciation, CO_2 saturation gradient and air–water fluxes are less than those of DO. DIC is used to accurately compute carbon mass balances. In the simplest possible scenario, ecosystem-level photosynthetic and respiration quotients (PQ_E and RQ_E) stoichiometrically link changes in DIC and DO. Aqueous CO_2 and its hydrated form H_2CO_3 are not differentiated, and are combined as CO_2. Bubbles in the figure only represent the relative magnitude of gas flux and do not indicate the formation of bubbles. DIC, dissolved inorganic carbon; DO, dissolved oxygen.

DIC. Empirical measurements, such as isotopic methods (Carvalho 2014), could provide ecosystem-level values, but cannot capture their potential variability over time (Berggren et al. 2012; Trentman et al. 2023). These other ecosystem processes jointly make it difficult to predict the PQ_E and RQ_E. Ultimately, we need a better understanding of the processes that control DIC cycling in rivers, which requires coupling time series measurements of DIC with models of inorganic carbon dynamics.

GPP and ER can be estimated from diel cycles of DIC after accounting for CO_2 equilibration with atmosphere. Development of models for DIC has been slower than for DO, however, likely due to the added complexity of inorganic carbon equilibria and lack of accurate, inexpensive, and easy to use in situ pCO_2 sensors. DIC models must account for CO_2 equilibria with HCO_3^- and CO_3^{2-} within the DIC pool, that is, carbonate buffering (Fig. 1). Many models have used CO_2 (pCO_2 converted to CO_2 using Henry's law constant) directly without accounting for the CO_2 equilibria (Wright and Mills 1967; Wolf and Olson 1974; Crawford et al. 2014), which neglects that fact that HCO_3^- is the dominant DIC species in circumneutral to alkaline rivers (Stets et al. 2017).

DIC metabolism models can be derived using the single-station (Kelly et al. 1983; Lynch et al. 2010) or two-station methods (Pennington et al. 2018), analogous to common practices with inferential DO models (Demars et al. 2015). Ideally for the single-station approach, the upstream reach should approximately follow the same diel pattern as measured at the sensor site. This behavior is more likely to be observed for DO because of its relatively rapid equilibration with the atmosphere, such that any heterogeneous process, for example, a tributary input, is erased over a relatively short reach. The reach length has been proposed to be estimated using $3v/K_{DO}$ (v, flow velocity; K_{DO}, gas exchange rate coefficient) (Reichert et al. 2009) which is the distance required for erasing 95% of upstream metabolic fluxes of DO. CO_2 gas exchange takes much longer to erase the upstream influence of metabolism on DIC, however, because the majority of DIC is in the form of HCO_3^- that buffers the effect of gas exchange on the rate of return to a CO_2 saturation state (Stets et al. 2017) (Fig. 1). The low equilibration rate with the atmosphere for DIC relative to DO suggests that the river "remembers" upstream variation in DIC over a much longer reach than that of DO, thereby preventing DO and DIC single-station models from representing the metabolic effects of the same reach. Two-station approaches can alleviate this problem because the influencing reach is explicitly defined by the two sensor locations (Hensley and Cohen 2016). The changes in DO or DIC in parcels of water as they pass between two measurement stations are calculated using the travel time. For a particular river section, the shorter time for DO to reach air–water equilibrium makes single- and two-station DO models generally agree unless a large discontinuity (e.g., dam or tributary) exists (Hall and Hotchkiss 2017). However, metabolism

estimates from the single-station DIC model could be influenced by the river processes well upstream of monitoring stations, which should be evaluated by comparing with estimates from the two-station DIC model.

Here, we explore how riverine metabolism estimated from DIC and DO differ. We hypothesized that the difference between DIC and DO metabolism is reflected by deviation of PQ_E from PQ, or RQ_E from RQ because multiple processes occur concomitantly that have different stoichiometries decoupling DIC and DO. Quantifying the difference should be aided by two-station modeling of both DIC and DO. We therefore (1) developed new DIC models that are based upon high-frequency time series of pCO_2 and account for carbonate buffering; (2) examined model capabilities of recovering parameters with simulated data; (3) tested modeling methods by comparing single- and two-station model fits and metabolism estimates in a mid-order river at three reaches; (4) examined relationships (PQ_E, RQ_E) between two-station DO and DIC metabolism; (5) used the two-station model to evaluate the relationship between both DO and DIC metabolism and CO_2 emissions.

Methods

Site descriptions

We deployed sensors in reaches along a 216-km section of the Upper Clark Fork River (Fig. 2a). The section of the river is a mid-order, open-canopied channel with several tributaries from mountainous headwaters that greatly contribute to the total discharge. The river is the site of extensive remediation due to contamination of floodplain sediments by the redistribution of mining byproducts from a major flood (Moore and Langner 2012). The filamentous green algae, *Claudophora glomerata*, blooms on the cobble riverbed. Benthic algal chlorophyll *a* can routinely exceed 100 mg m^{-2}, motivating development of strategies to manage eutrophication by reducing external nutrient loading (Dodds et al. 1997; Suplee et al. 2012).

This study focused on three reaches: Garrison, Jens, and Milltown, which are 45, 90, and 200 km from the river's origin, respectively (Fig. 2a; Supporting Information Table S1; Fig. S1). We selected sites to avoid reaches with substantial net gains from groundwater and surface tributary inputs. In 2020, sensors were deployed at three sites along Garrison starting ~ 4 km downstream from the Deer Lodge waste water treatment plant (WWTP) and ~ 11 km downstream from the town of Deer Lodge (Fig. 2b; Supporting Information Fig. S1). We refer to these sites as "up," "mid," and "down" relative to river flow, and use a hyphen to denote reaches for two-station models, for example, up–mid indicates the reach from upstream to middle sites. The distance was ~ 7 km for up–down, and ~ 3 km for up–mid. In 2019, sensors were deployed at two sites (up and down) separated by ~ 6 km along Jens (Fig. 2c; Supporting Information Fig. S1). Two deployments were performed in Milltown in September and December, 1999, before the Milltown Dam was removed (Fig. 2d; Supporting Information Fig. S1). The September deployment occurred in a 9-km reach which was 1-km downstream from the Milltown Dam. In December, the upstream site was moved downstream to shorten the reach to ~ 6 km. This old dataset was never published in peer-reviewed literature (Reynolds 2001) and is included here to provide a case study of a distinct upstream heterogeneity in river chemistry.

Data collection

Sensor deployments

For Garrison and Jens, we installed sensors for CO_2 (SAMI-CO_2, Sunburst Sensors), DO (miniDOT, PME) and conductivity (HOBO-U24-001, Onset) at each site, which sampled at 15-min intervals (data summarized in Table 1). Water temperature was measured by all sensors with an agreement of $\pm$ 0.2°C. For Milltown, DO and conductivity were recorded by a multiparameter sonde (YSI model 6000) with the same CO_2 sensor as in other reaches. The SAMI-CO_2 measures pCO_2 by allowing ambient river pCO_2 to equilibrate across a gas-permeable membrane with a colorimetric pH indicator solution (DeGrandpre et al. 1995). SAMI-CO_2 sensors were calibrated in a temperature-controlled tank with CO_2 quantified using an infrared gas analyzer (LI-COR, LI-840A). The pH indicator optical absorbances are recorded in situ, which enables calculation of water pCO_2. Calibration uncertainties were 1%, estimated by deploying three SAMI-CO_2 sensors at the same river location for a 24-h period. Oxygen sensors were calibrated by measuring oxygen-free water prepared by adding excess sodium persulfate and were also initially co-located in the river with an agreement of 0.8%. The conductivity sensor was calibrated with 1000 μS cm^{-1} conductivity standards (RICCA Chemical Company), and the YSI conductivity sonde was calibrated with factory supplied standards. While no drift was identified for the miniDOT, prior and post calibrations suggest that the YSI DO sondes in the two 1999 deployments drifted by 6% to 15% (Reynolds 2001). A linear correction was applied as suggested by the manufacturer.

Discrete samples were also collected over the deployments for sensor quality assurance. DO was measured in discrete samples by Winkler titration (Carpenter 1965). Discrete pCO_2 was calculated from spectrophotometric pH (Lai et al. 2016) and alkalinity (A_T) determined by titration (Young et al. 2022). We found that the time series did not have systematic offsets between upstream and downstream sites. More descriptions of sensor data validation are presented in the sensor time-series plots (Supporting Information Figs. S2, S3). A_T from discrete samples was also used to drive DIC metabolism models, as described below.

Supporting data

We collected the meteorological and hydrological data necessary for the metabolism models. Mean atmospheric CO_2 mole fraction was 360 ppm in 1999 and 414 ppm in 2019 and

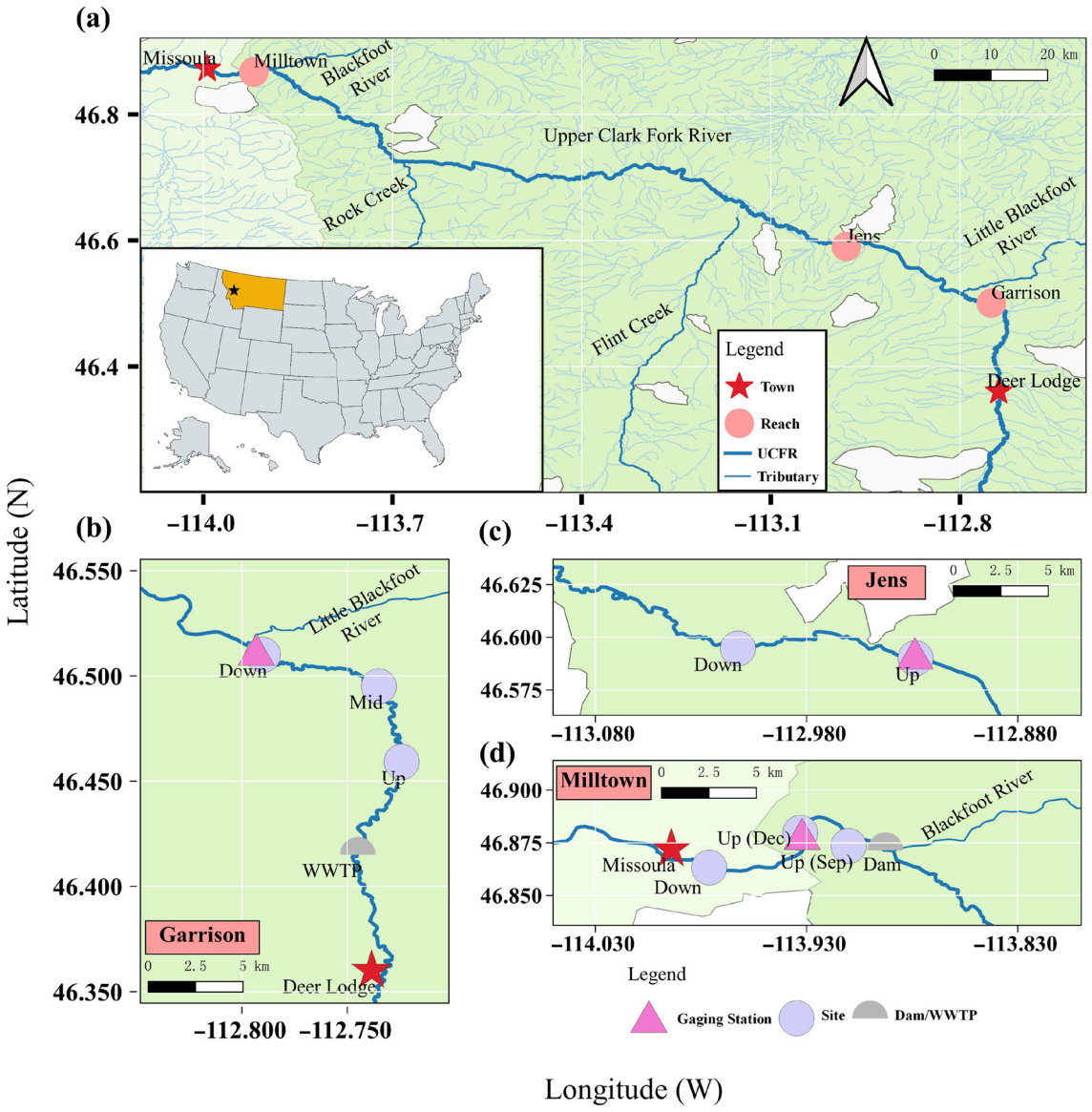

Fig. 2. Map of the Upper Clark Fork River showing locations of reaches and sites (Supporting Information Table S1). (**a**) An overview of the river, tributaries and the three reaches, Garrison, Jens, and Milltown. (**b**) An enlarged view of Garrison with three sites, up, mid, down, and U.S. Geological Survey (USGS) gaging station #12324400. The river flows by the town of Deer Lodge and its Waste Water Treatment Plant (WWTP). (**c**) Jens with up and down sites and USGS gaging station #12324680. (**d**) Milltown with upstream September (Sep), upstream December (Dec), and down. The gaging station #12340500 near up (Dec) was located ~ 4 km downstream from the Milltown Dam.

2020 measured at Mauna Loa Observatory (Andrews et al. 2020), which were used to calculate atmospheric pCO_2 based on local barometric pressure after correcting for water vapor pressure (Dickson et al. 2007). For Garrison in 2020 and Jens in 2019, we obtained local barometric pressure and photosynthetically active radiation (PAR) from a MesoWest station (mesowest.utah.edu) near Deer Lodge (Fig. 2b). For Milltown in 1999, we obtained barometric pressure from the NOAA National Climatic Data Center in Missoula, Montana, and monitored PAR using an underwater LI-COR quantum sensor (model LI-192SA). River discharge was downloaded from nearby U.S. Geological Survey (USGS) gaging stations (Fig. 2; Supporting Information Table S1). To obtain real-time depth data, we compiled results from 29 channel morphology surveys in the Upper Clark Fork River. Each survey had 20 transects over a > 3 km reach with 10 evenly spaced depth measurements at every transect. We derived an empirical relationship using values from the 29 surveys of discharge and depth (Carter et al. unpubl.) that allows depth time series to be back calculated from discharge (Table 1). We measured travel time for the Garrison reach by performing a Rhodamine water tracer release experiment and identifying the timing of

Table 1. Three reaches and all measured variables, expressed as mean ± one standard deviation. All sensor measurements, discharge and depth were obtained at 15-min intervals. The Garrison reach had two subsections with travel time (τ) of 75 and 105 min for up–mid and mid–down, respectively. A_T measurements were based on discrete samples with a total number of 41 for Garrison, 22 for Jens, 28 for Milltown (September), and 27 for Milltown (December). Number of samples for sites at the same reach was nearly identical. More data descriptions are given in Supporting Information 2 (Supporting Information Figs. S2, S3).

Reach	Days	τ (min.)	pCO_2 (μatm)	DO (μmol L^{-1})	A_T (μmol L^{-1})	Temp. (°C)	Discharge (m^3 s^{-1})	Depth (m)	Cond. (μS cm^{-1})
Garrison	47	75 + 105	627 ± 300	292 ± 66	3179 ± 58	13 ± 3	5.7 ± 0.7	0.55 ± 0.01	482 ± 7
Jens	50	180	711 ± 300	268 ± 46	3028 ± 92	16 ± 3	10 ± 2.9	0.63 ± 0.04	418 ± 13
Milltown (Sep)	14	255	349 ± 92	326 ± 30	2727 ± 27	11 ± 2	36 ± 1.8	1.16 ± 0.03	255 ± 9
Milltown (Dec)	10	150	351 ± 47	398 ± 14	2662 ± 30	1.7 ± 0.8	40 ± 1.4	1.23 ± 0.03	266 ± 5

DO, dissolved oxygen; pCO_2, partial pressure of CO_2.

peak fluorescence at each site. For Jens and Milltown, we estimated their travel time by identifying spikes in conductivity that coincided with distinct discharge events (Table 1).

Metabolism models

Single-station models

We used the open-source R package *streamMetabolizer* (Appling et al. 2018) as the single-station DO model. The *streamMetabolizer* package uses a DO mass balance that is a function of ecosystem metabolic fluxes and gas exchange:

$$C_{\mathrm{DO},t+\Delta t} = C_{\mathrm{DO},t} + \Delta t\left[\left(\frac{\overline{P}_{\mathrm{DO}}}{\overline{z}}\cdot\frac{L_t}{\overline{L}}\right) - \left(\frac{\overline{R}_{\mathrm{DO}}}{\overline{z}}\right) + K_{\mathrm{DO},t}\left(C^*_{\mathrm{DO},t} - C_{\mathrm{DO},t}\right)\right], \quad (1)$$

where $C_{\mathrm{DO},t}$ and $C_{\mathrm{DO},t+\Delta t}$ are the modeled DO at time t and $t+\Delta t$, and Δt is the sensor measurement interval (Supporting Information 3; Table S2). $\overline{z}$ is reach-averaged water depth (m). $\overline{P}_{\mathrm{DO}}$ and $\overline{R}_{\mathrm{DO}}$ are GPP and ER inferred from DO ($\mathrm{GPP_{DO}}$ and $\mathrm{ER_{DO}}$, mmol m^{-2} d^{-1}). We assumed a linear relationship to derive $\overline{P}_{\mathrm{DO}}$ from PAR variation, modeled as the ratio of photosynthetic photon flux density at time t (L_t) over its daily mean ($\overline{L}$, μmol m^{-2} d^{-1}), which works well for most rivers (Hall et al. 2016). The gas exchange flux uses the saturation concentration of DO at time t as a function of water temperature and local barometric pressure $\left(C^*_{\mathrm{DO},t}\right)$ (Garcia and Gordon 1992). $K_{\mathrm{DO},t}$ is a time-variant, temperature-dependent gas exchange coefficient $\left(\mathrm{d}^{-1}\right)$ for DO, which is converted from a standard gas exchange coefficient with a Schmidt number of 600 (K_{600}) (Raymond et al. 2012).

The *streamMetabolizer* package uses Bayesian inference of a state space hierarchical model to sample posterior probability distributions of the parameters (Appling et al. 2018). The state space hierarchical model estimates observation error and process error assumed in the DO time series. Observation errors are random noise directly added to the modeled data at each point, for example, sensor imprecision. Process errors occur when models do not accurately quantify underlying processes (i.e., metabolism and gas exchange). For example, ER is assumed to be constant but may vary between day and night (Hotchkiss and Hall 2014). Process errors are added for each time step and persist over time. We considered both types of errors. The *streamMetabolizer* allows users to pool K_{600} against discharge to reduce equifinality (i.e., three parameters covary to achieve good fits to the DO data), but we chose not to use the $K_{600} \sim$ discharge relationship because the discharge variation was < 30% during the deployments (Table 1; Supporting Information Fig. S2). We used coefficient of determination (R^2) between modeled and observed data for assessing the within-day quality of fitting.

We also derived a single-station model for DIC metabolism,

$$C_{\mathrm{DIC},t+\Delta t} = C_{\mathrm{DIC},t} + \Delta t\left[-\left(\frac{\overline{P}_{\mathrm{DIC}}}{\overline{z}}\cdot\frac{L_t}{\overline{L}}\right) + \frac{\overline{R}_{\mathrm{DIC}}}{\overline{z}} + K_{\mathrm{CO_2},t}\cdot K_{\mathrm{H},t}\left(P^*_{\mathrm{CO_2},t} - P_{\mathrm{CO_2},t}\right)\right], \quad (2)$$

where DIC is used to construct the mass balance equation rather than pCO_2 due to carbonate equilibria (Stets et al. 2017), while pCO_2 is only used to calculate gas exchange flux. $\overline{P}_{\mathrm{DIC}}$ and $\overline{R}_{\mathrm{DIC}}$ are GPP and ER inferred from DIC ($\mathrm{GPP_{DIC}}$ and $\mathrm{ER_{DIC}}$, mmol m^{-2} d^{-1}). $C_{\mathrm{DIC},t+\Delta t}$ and $C_{\mathrm{DIC},t}$ are modeled DIC at time t and $t+\Delta t$. $P_{\mathrm{CO_2},t}$ and $P^*_{\mathrm{CO_2},t}$ are river pCO_2 and local atmospheric pCO_2 at time t, respectively. $K_{\mathrm{H},t}$ is the temperature dependent solubility of CO_2 (Weiss 1974). $P_{\mathrm{CO_2},t}$ is calculated by $C_{\mathrm{DIC},t}$, A_T and temperature for each time step by solving mass balance, alkalinity balance and equilibrium equations based on deprotonation reactions of dissolved CO_2 and HCO_3^- (details in Supporting Information 4). Comparing the signs in DO (Eq. 1) and DIC (Eq. 2) models, we enforced the budgetary sign conventions with the stoichiometric coefficients rather than the process rates for multi-metabolite modeling and later deriving $\mathrm{PQ_E}$ and $\mathrm{RQ_E}$.

We assume protolytic nutrients (e.g., phosphate), calcite mineralization, and organic acids have negligible contributions to A_T in the Upper Clark Fork River. Biological CO_2 uptake and release and air–water CO_2 exchange do not change A_T. A_T can vary on short-term (< diel) scales due to processes not included in this model, such as evapotranspiration (ET) that drives diel cycles of groundwater inputs (Shangguan et al. 2021). While ET could also contribute to DIC dynamics, we have insufficient data to parameterize the more complex model of diel changes in groundwater influence. Instead, using a constant A_T to calculate DIC from pCO_2 maximizes contributions of metabolism and gas exchange to the DIC mass balance and minimizes that of ET. We performed simple numerical experiments to evaluate the error introduced by assuming the use of a constant A_T (Supporting Information 5; Table S3; Fig. S4). Three scenarios were simulated to represent different effects of ET and calcite precipitation. The results demonstrated the varying A_T should change the metabolism estimates by < 10% in the Upper Clark Fork River. We also found that ± 5% systematic errors in A_T had negligible effects on metabolism estimates.

We used K_{600} derived from *streamMetabolizer* for all other metabolism analyses to remove the confounding influence of variations in K_{600} on DIC vs. DO metabolism estimates. The DIC model becomes essentially a two-parameter inverse model (i.e., GPP_{DIC} and ER_{DIC}) after fixing K_{600} (Eq. 2). $K_{CO_2,t}$, the gas exchange coefficient for CO_2 at time t, is scaled to K_{600} with Schmidt number coefficients (Jähne et al. 1987). Uncertainty of K_{600} inferred from different DO metabolism models does not affect estimates of the DO and DIC stoichiometry (Supporting Information 6; Tables S4, S5; Figs. S5, S6).

DIC metabolism models were implemented in C++. Interfaces to the models including maximum likelihood inversion tools were developed in R (R Core Team 2018). We used a Maximum Likelihood Estimation (MLE) function (*optim* function in R) to find GPP_{DIC} and ER_{DIC} by assuming residuals between $P_{CO_2,t}$ and measured pCO_2 are independent and normally distributed. MLE saves the runtime via a single realization and does not have equifinality problems for only two free parameters (GPP and ER).

Two-station models

Two-station models simulate changes in solute concentrations (e.g., DO) in parcels of water traveling a defined reach between upstream and downstream monitoring stations (Hall and Tank 2005; Hall et al. 2016; Payn et al. 2017). The two-station DO and DIC models are presented in Eqs. 3 and 4, respectively, based on the same processes as those in single-station models:

$$C_{DO,t+\tau} = \frac{C_{DO,t} + \frac{\overline{P}_{DO}}{\overline{z}} \cdot \frac{\overline{L}_\tau}{\overline{L}}\tau - \frac{\overline{R}_{DO}}{\overline{z}}\tau + \frac{\overline{K}_{DO,\tau}}{2}\tau\left(C^*_{DO,t} - C_{DO,t} + C^*_{DO,t+\tau}\right)}{1 + \frac{\overline{K}_{DO,\tau}}{2}\tau}, \quad (3)$$

$$C_{DIC,t+\tau} + \overline{K}_{CO_2,\tau}\frac{K_{H,t+\tau} \cdot P_{CO_2,t+\tau}}{2}\tau = C_{DIC,t} - \frac{\overline{P}_{DIC}}{\overline{z}} \cdot \frac{\overline{L}_\tau}{\overline{L}}\tau + \frac{\overline{R}_{DIC}}{\overline{z}}\tau + \overline{K}_{CO_2,\tau}\left(\frac{K_{H,t}\left(P^*_{CO_2,t} - P_{CO_2,t}\right)}{2} + \frac{K_{H,t+\tau} \cdot P^*_{CO_2,t+\tau}}{2}\right)\tau, \quad (4)$$

where τ is the travel time between stations and t is the time at the upstream site (Supporting Information Table S2). In Eq. 3, $C_{DO,t+\tau}$ and $C^*_{DO,t+\tau}$ are downstream modeled DO concentration and atmospheric saturation concentration at time $t+\tau$, respectively. $C_{DO,t}$ and $C^*_{DO,t}$ are corresponding upstream values at time t. In Eq. 4, $P_{CO_2,t+\tau}$ and $C_{DIC,t+\tau}$ are modeled downstream pCO_2 and DIC, which are solved simultaneously constrained by A_T (Supporting Information 4). $P_{CO_2,t}$ and $C_{DIC,t}$ refer to upstream values of pCO_2 and DIC. As identified by discrete sample data, the downstream A_T is the same as the upstream A_T for $C_{DIC,t}$. $P^*_{CO_2,t+\tau}$ and $K_{H,t+\tau}$ are downstream atmospheric pCO_2 and the solubility constant, respectively, while $P^*_{CO_2,t}$ and $K_{H,t}$ are corresponding upstream values.

A Crank Nicolson approximation was applied over the period of τ to average variables at upstream and downstream stations for prediction (Supporting Information Table S2), which is commonly employed for two-station models (e.g., Payn et al. 2017). For any parcel of water traveling through the reach, PAR is approximated as the average of upstream and downstream PAR offset by τ ($\overline{L}_\tau$). We also applied the same approximation for the DO and CO_2 gas exchange coefficient ($\overline{K}_{DO,\tau}$ and $\overline{K}_{CO_2,\tau}$).

To ensure consistency in K_{600} among different model analyses, we did not estimate K_{600} as a free parameter for two-station models. Rather, we used K_{600} based on *streamMetabolizer* estimates (Eq. 1) at the downstream site, leaving GPP_{DO} and ER_{DO} (Eq. 3), or GPP_{DIC} and ER_{DIC} (Eq. 4) as the only two estimated parameters. The Milltown reach is an exception where the single-station model did not fit to the data (shown later), so we allowed the two-station DO model to infer K_{600} (Eq. 3) for this reach only, which was subsequently imported into the two-station DIC model (Eq. 4). We employed MLE to find parameters by assuming residuals between measured downstream DO and modeled $C_{DO,t+\tau}$ (Eq. 3), or measured downstream pCO_2 and modeled $P_{CO_2,t+\tau}$ (Eq. 4) are independent and normally distributed.

Model testing by simulated data with errors

We tested the models by simulating pCO_2 and DO data, adding errors to the data and estimating the ability of the model to recover prespecified parameters. For both single- and two-station models, we assigned 150 mmol m^{-2} d^{-1} to GPP_{DO} and GPP_{DIC}, 225 mmol m^{-2} d^{-1} to ER_{DO} and ER_{DIC}, 10 d^{-1} to

K_{600}. Net ecosystem production (NEP) for both DO (NEP_{DO}) and DIC (NEP_{DIC}) were set to -75 mmol m^{-2} d^{-1}. These parameter values are typical for the Upper Clark Fork River (Carter et al. unpubl.). For the single-station model (Eqs. 1, 2), we extracted measured depth, temperature, and light at the downstream site, Garrison on August 28, 2020 to simulate $C_{DO,t}$ and $P_{CO_2,t}$. For the two-station model (Eqs. 3, 4), we started with a 46-d pCO_2 and DO time series at the upstream site, Garrison that provides a natural upstream boundary condition (i.e., measured $C_{DO,t}$ and $P_{CO_2,t}$ at upstream). We used $\tau = 3$ h (the travel time for up–down at Garrison, Table 1) to simulate downstream pCO_2 and DO data (i.e., $C_{DO,t+\tau}$ and $P_{CO_2,t+\tau}$).

Error structures differ in simulated diel cycles for single- and two-station models (equations in Supporting Information 7). All errors are normally distributed around a mean of zero. For pCO_2, observation errors had one standard deviation (SD) of 10 μatm based on field co-deployment data, and process errors had a SD of 960 μatm d^{-1} (10 μatm for Δt). For DO, observation errors had a SD of 2 μmol L^{-1}, and process errors had a SD of $\pm$ 192 μmol L^{-1} d^{-1} the same as the upper bound values in Appling et al. (2018). We added both types of errors to the simulated data for single-station models, but only observation errors for two-station models. The two-station model calculates the changes between upstream and downstream data (DO or DIC), thereby minimizing the process errors. In addition, we evaluated potential error in K_{600} that propagates systematically into GPP and ER because DIC models used K_{600} inferred by DO models. An error ranging from -2 to 2 at an interval of 1 d^{-1} was applied to examine the model sensitivity to K_{600} considering the range of inferred K_{600} by DO models (Supporting Information Fig. S5).

Simulated data with added errors were treated as "observed" data to understand how the error influences parameter estimates. For single-station models, the procedures of simulation and inference were repeated for 50 realizations of the same diel cycle, but with new errors for every simulation to constrain the uncertainty. Uncertainty was bracketed by the maximum and minimum estimates from the ensemble of realizations. For two-station models, we calculated the uncertainty based on 46 estimates of GPP, ER, and NEP from realizations of the 46-d time series. Observation errors were regenerated for each day.

Comparison of single- and two-station models

We used regressions between single- and two-station model results for both DO and DIC data to illustrate where they provide similar or disparate information on river metabolism. Uncertainties of metabolism estimates were present for both single- and two-station models. This comparison evaluated the uncertainties primarily driven by reach heterogeneity and other factors such as τ and data inaccuracy. For the Garrison reach, the three sites yielded three sub-reaches for two-station models (up–down, up–mid, and mid–down). Intercomparison of the three sub-reaches further verified the two-station model results and the effect of τ (Supporting Information 8; Table S6; Fig. S7). We used reduced major axis (RMA) regressions to account for the influence of errors on both the horizontal and vertical axes because of the symmetric nature of comparing two methods (Warton et al. 2012).

Stoichiometry, metabolism, and CO_2 emissions

We quantified PQ_E and RQ_E using DO and DIC metabolism estimates. For each deployment, we performed ordinary least squares (OLS) regressions between two stations GPP_{DO} and GPP_{DIC}, ER_{DO} and ER_{DIC} with intercepts fixed to 0 mmol m^{-2} d^{-1}. PQ_E is the slope $\pm$ one standard error for GPP, and RQ_E is the inverse of the slope for ER. Single-station models are not discussed here because one of our findings is that errors in single-station DIC results were large, generating large scatter in PQ_E and RQ_E. PQ_E and RQ_E were also calculated by using individual estimates from two-station models each day:

$$PQ_E = \frac{GPP_{DO}}{GPP_{DIC}}, \quad RQ_E = \frac{ER_{DIC}}{ER_{DO}}. \tag{5}$$

PQ_E and $RQ_E > 1$ indicates $GPP_{DO} > GPP_{DIC}$ and $ER_{DO} < ER_{DIC}$ on a molar basis, respectively. We also used RMA regressions to explore the difference between NEP_{DO} and NEP_{DIC} that is driven by a combined effect of PQ_E and RQ_E.

NEP_{DIC} and daily CO_2 emissions were compared in OLS regressions to illustrate where ecosystem metabolism may be the primary driver of CO_2 emissions. Daily CO_2 emissions were obtained by integrating air–water equilibration terms in Eq. 4 at every measurement step for each day: $\overline{K}_{CO_2,\tau}\left(K_{H,t}\left(P_{CO_2,t} - P^*_{CO_2,t}\right)/2 + K_{H,t+\tau}\left(P_{CO_2,t+\tau} - P^*_{CO_2,t+\tau}\right)/2\right)$. The same regression was performed using NEP_{DO} for comparison. The relationship of daily CO_2 emission to NEP suggests that in-stream CO_2 production contributed to CO_2 levels. A negative NEP_{DIC} means net respiration, that is, DIC and CO_2 addition, and a positive NEP_{DIC} means net photosynthesis, that is, DIC and CO_2 reduction. The regression intercept, or zero NEP_{DIC}, quantifies the external source of CO_2 from upstream of the reach that raised mean levels of CO_2 above atmospheric saturation. Generally, we expect that higher $P_{CO_2,t}$ indicates more CO_2 imported from upstream, like those observed at Garrison and Jens (mean values in Table 1). Note the external CO_2 source included CO_2 produced in upstream sections and exported to the reach and groundwater DIC inputs (Hotchkiss et al. 2015).

Results

Results from this work assessed the utility of river metabolism models based on DIC dynamics. Simulation experiments evaluated how error structures in diel data and systematic errors in K_{600} affected parameter estimates. Comparison of

single- and two-station models illustrates how the river reach linked to a given metabolism estimate may vary between the methods. Finally, comparison of metabolism estimates from DO and DIC models revealed variations in ecosystem-level stoichiometry.

Estimating metabolism from simulated diel cycles

At the baseline K_{600} of 10 d^{-1}, metabolism estimates from simulated diel cycles demonstrated that the single-station models of both DO and DIC resulted in more uncertainty (20–40 mmol m^{-2} d^{-1}) in recovered parameters (Fig. 3a,b) than two-station models (Fig. 3c,d). The difference comes from process errors that were explicitly applied to single-station models as explained above (equations in Supporting Information 7). Observation errors simply added noise to the recovered parameters, the magnitude of which did not differ between single- and two-station models (i.e., note the similar size of the error bars in Fig. 3a,c or Fig. 3b,d). The assigned values in observation errors had greater effects on DO than DIC as shown by comparing a and b in Fig. 3.

The DO and DIC models reflected different levels of error in metabolic parameters caused by errors in K_{600} (Fig. 3). We focused here on two-station models to remove effects of process error. Although error in GPP_{DO} and ER_{DO} (Fig. 3c) was > 2 times more sensitive to error in K_{600} than GPP_{DIC} and ER_{DIC} (Fig. 3d), NEP_{DO} was relatively insensitive to the K_{600} error (Fig. 3c). The error in NEP_{DIC} was stronger than that in NEP_{DO} (Fig. 3d) because the error in GPP_{DO} and ER_{DO} tracked together but the error in GPP_{DIC} and ER_{DIC} differed. The difference between the DO and DIC parameters points to the different diel variations in air–water exchange fluxes for DO and CO_2. The instantaneous gas exchange flux was smaller for CO_2 than DO (Fig. 1). CO_2 supersaturation was observed for nearly at all times at Garrison with greater emissions at night than during the day (Supporting Information Fig. S2a1). Conversely, DO efflux and influx between daytime and

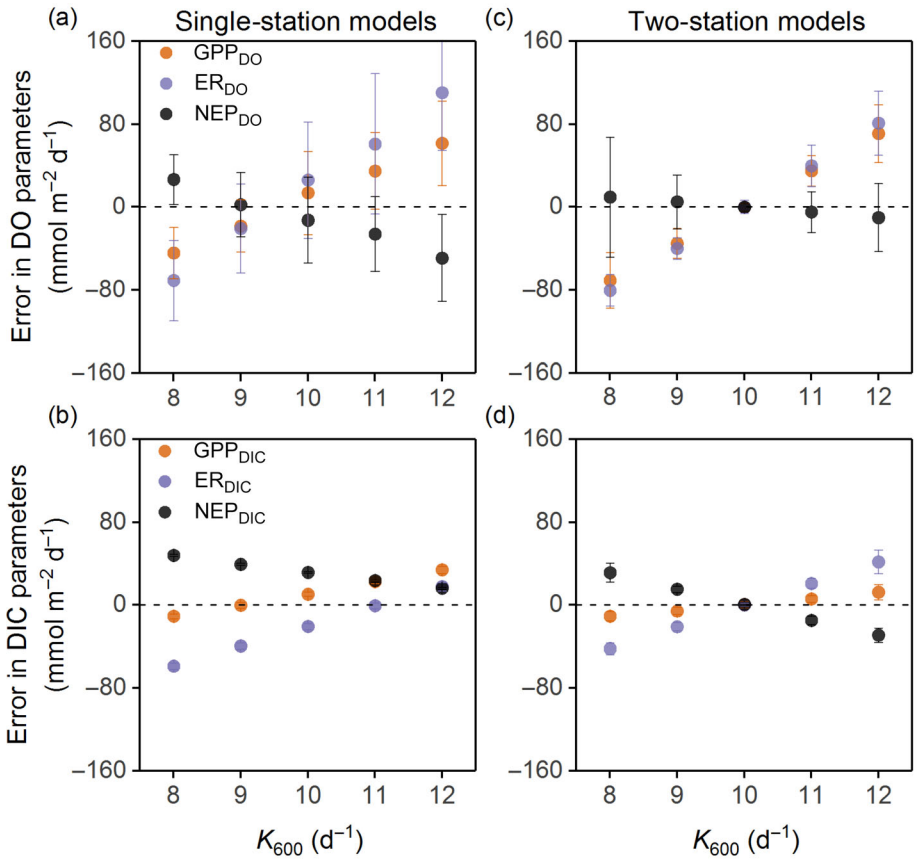

Fig. 3. Errors in K_{600} and diel pCO_2 and DO data affected estimation of GPP (orange), ER (purple), and NEP (black) for single-station (left) and two-station (right) models. Error bars represent the uncertainty quantified by the range of estimates. For all simulations, GPP = 150 mmol m^{-2} d^{-1}, ER = 225 mmol m^{-2} d^{-1}, and K_{600} = 10 d^{-1}. Observation errors are 0 ± 2 μmol L^{-1} for DO and 0 ± 10 μatm for pCO_2. Process errors are 0 ± 192 μmol $L^{-1}d^{-1}$ for DO and 0 ± 960 μatm d^{-1} for pCO_2. However, only observation errors were applied to the two-station models as explained in the text and Supporting Information 7. Each panel corresponds to (**a**) single-station DO model, (**b**) single-station DIC model, (**c**) two-station DO model, and (**d**) two-station DIC model. For DIC models, uncertainties are small and not visible on the *y*-axis scale. DIC, dissolved inorganic carbon; DO, dissolved oxygen; ER, ecosystem respiration; GPP, gross primary production; NEP, net ecosystem production; pCO_2, partial pressure of CO_2.

nighttime were relatively close because DO was symmetrically distributed around saturation (Supporting Information Fig. S2b1). Importantly, the two-station DIC model recovered the parameters successfully given an accurate K_{600} (Fig. 3d). By fixing the same K_{600} for DO and DIC models, error in K_{600} interferes with the comparison of DO and DIC metabolism to an even lesser extent.

Comparing single- and two-station metabolism estimates

Fits of single-station models to data generally captured the major features of the DO and pCO_2 metabolite signals at Garrison and Jens (modeled vs. measured data, $R^2 = 0.94$), but failed to follow observations at Milltown ($R^2 = 0.60$) (Fig. 4 upper right two rows). At Garrison and Jens, the relatively small residual errors were highly autocorrelated in DO and pCO_2 model fits (not shown), suggesting subtle structural errors in the models, for example, offset of light due to diel shading (Yard et al. 2005). The lack of ability to fit single-station models to the dam-influenced data with double peak or dip structures (Fig. 4; Supporting Information Fig. S3) led to ecologically unreasonable metabolic estimates for both DO and DIC. Accordingly, we excluded these datasets from further analysis.

Two-station model fits to the concentration change in parcels traveling the reach demonstrated reasonable model behavior in all three reaches (Fig. 4 lower two rows). The most accurate model fits ($R^2 = 0.95$) occurred in the Garrison up–down and Jens reaches when daily variation in metabolites

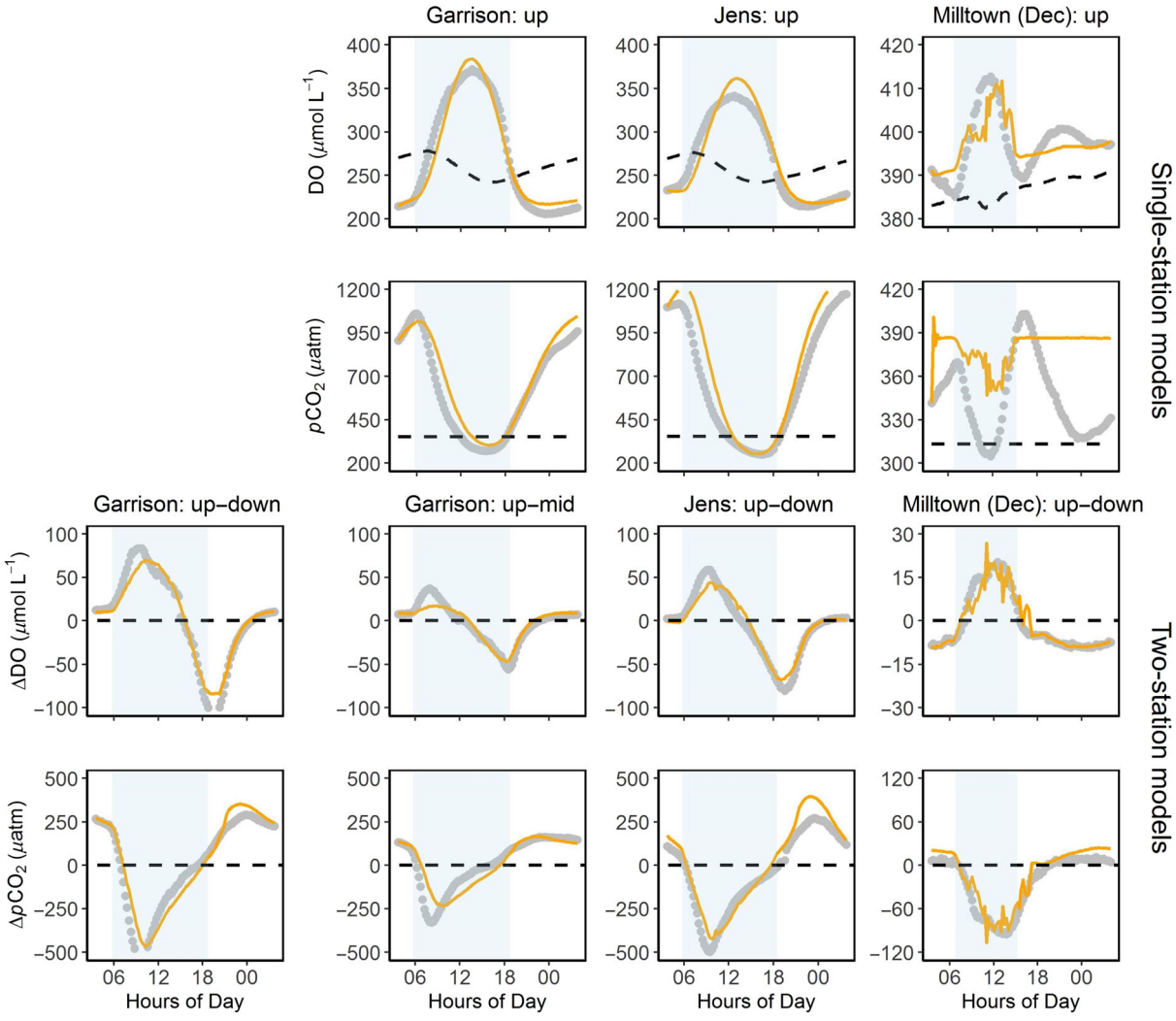

Fig. 4. Examples of model fits (orange lines) to observed data (gray points). Shaded areas indicate photoperiods (local time). For the single-station DO or DIC model (top two rows), dashed lines are DO solubility or atmospheric pCO_2. For the two-station DO or DIC model (bottom two rows), dashed lines are zero lines. In the Garrison reach, up–down and up–mid differ by travel time. Dates for the example data at three reaches are September 4, 2020, August 28, 2019, and December 13, 1999, respectively. Note that the Milltown panels have a different scale. DIC, dissolved inorganic carbon; DO, dissolved oxygen; pCO_2, partial pressure of CO_2.

was largest. The shorter distance for the Garrison up–mid ($R^2 = 0.85$) had smaller changes in metabolite concentrations compared to Garrison up–down, which led to more uncertainty in inference of model parameters (more details in Supporting Information 8; Table S6; Fig. S7). The Garrison mid–down, however, displayed comparable uncertainty to that observed for the longer up–down, supporting the quality of sensor data and two-station modeling. At Milltown, the two-station model greatly diminished the delayed peak for DO and dip for pCO_2 ($R^2 = 0.92$), but weak diel signals (Supporting Information Fig. S3) made it difficult to infer parameters.

The single- and two-station inferences of metabolism from DO data were similar, yet the single- and two-station inferences from DIC differed strongly. The RMA regressions between single- and two-station approaches showed that the DIC metabolism estimates between the two approaches had higher chances of large discrepancy than DO (Fig. 5; Fig. S8; Table S7 in Supporting Information 9). The discrepancy between the two approaches was more evident in Garrison (Fig. 5a,b) than Jens (Fig. 5c,d). Generally, the R^2 increased from upstream to downstream sites for both reaches, suggesting progressively reduced influence of upstream heterogeneity (Fig. 5b,d). At Garrison, for GPP_{DO} and ER_{DO}, slopes < 1 were associated with non-zero intercepts (Supporting Information Table S7; Fig. S8a,c). For GPP_{DIC}, the slopes < 1 for all sites (Fig. 5a), and single-station GPP_{DIC} stayed nearly constant and were approximately two thirds of the two-station GPP_{DIC} (Supporting Information Fig. S8b). Both GPP_{DIC} and ER_{DIC} had low R^2 at Garrison (Fig. 5b). At Jens, the comparison for GPP_{DIC} and ER_{DIC} improved considerably, evident by higher R^2 and slopes close to unity (Fig. 5c,d), indicating Jens had less upstream heterogeneity compared to Garrison. To summarize, at times parameters derived by single- and two-station approaches were dissimilar based either on DO or DIC data, with discrepancy between values more likely when based on DIC.

DO and DIC metabolism differed

The DO and DIC metabolism consistently differed for all three reaches. Two-station PQ_E were 1.67 ± 0.06, 1.95 ± 0.09, and 1.45 ± 0.06 at Garrison, Jens, and Milltown, respectively (Fig. 6a–c), meaning $GPP_{DO} > GPP_{DIC}$ for all three reaches (Eq. 5). PQ_E ranged from 0.8 to 2.8 among individual (daily) estimates. GPP_{DO} increasingly deviated from GPP_{DIC} as GPP magnitude increased, with daily PQ_E covarying with values of daily integrated light (Supporting Information 10; Fig. S9a). RQ_E were 0.84 ± 0.02, 0.80 ± 0.02, and 1.45 ± 0.41 at Garrison,

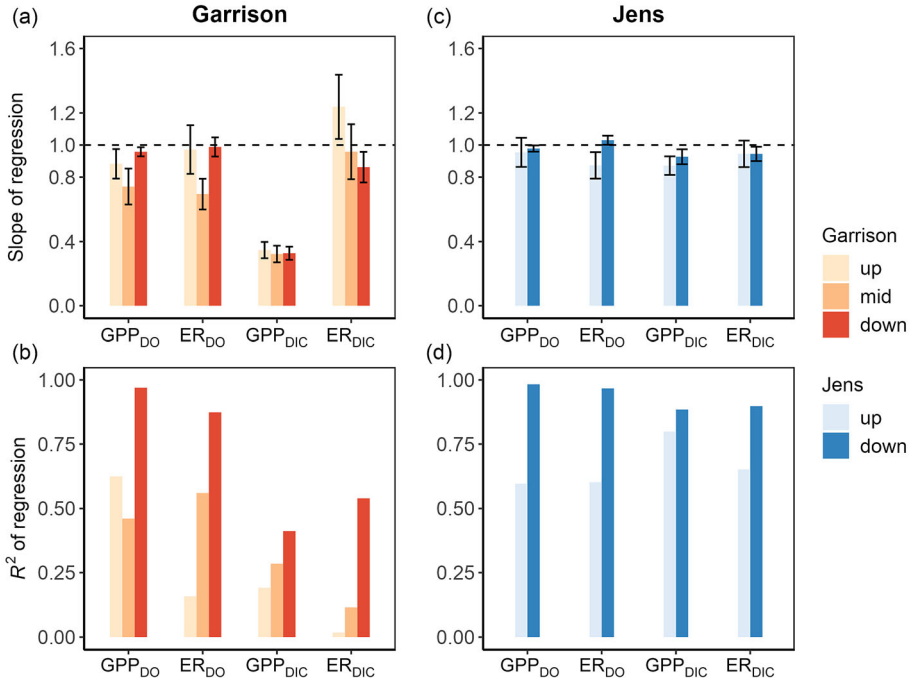

Fig. 5. Regression results for two-station up–down (*x*-axis) vs. single-station (up, mid, or down) (*y*-axis). Data and one-to-one plots are shown in Supporting Information Table S7 and Fig. S8, respectively. These results revealed that DIC models likely had larger discrepancy between single and two-station approaches than DO models. For each panel, data are grouped by parameters: GPP_{DO}, ER_{DO}, GPP_{DIC}, and ER_{DIC}. Two-station up–down on the *x*-axis was compared to single-stations via RMA regression for both reaches. Sites at Garrison are indicated by red gradient color (up, mid, down), and sites at Jens are indicated by blue gradient color (up, down). Top two panels: slope of regression at Garrison (**a**) and Jens (**c**). Error bars represent one standard error of the regression slope, and dashed lines represent values of one. Bottom two panels: R^2 of regression at Garrison (**b**) and Jens (**d**). DIC, dissolved inorganic carbon; DO, dissolved oxygen; ER, ecosystem respiration; GPP, gross primary production; RMA, reduced major axis.

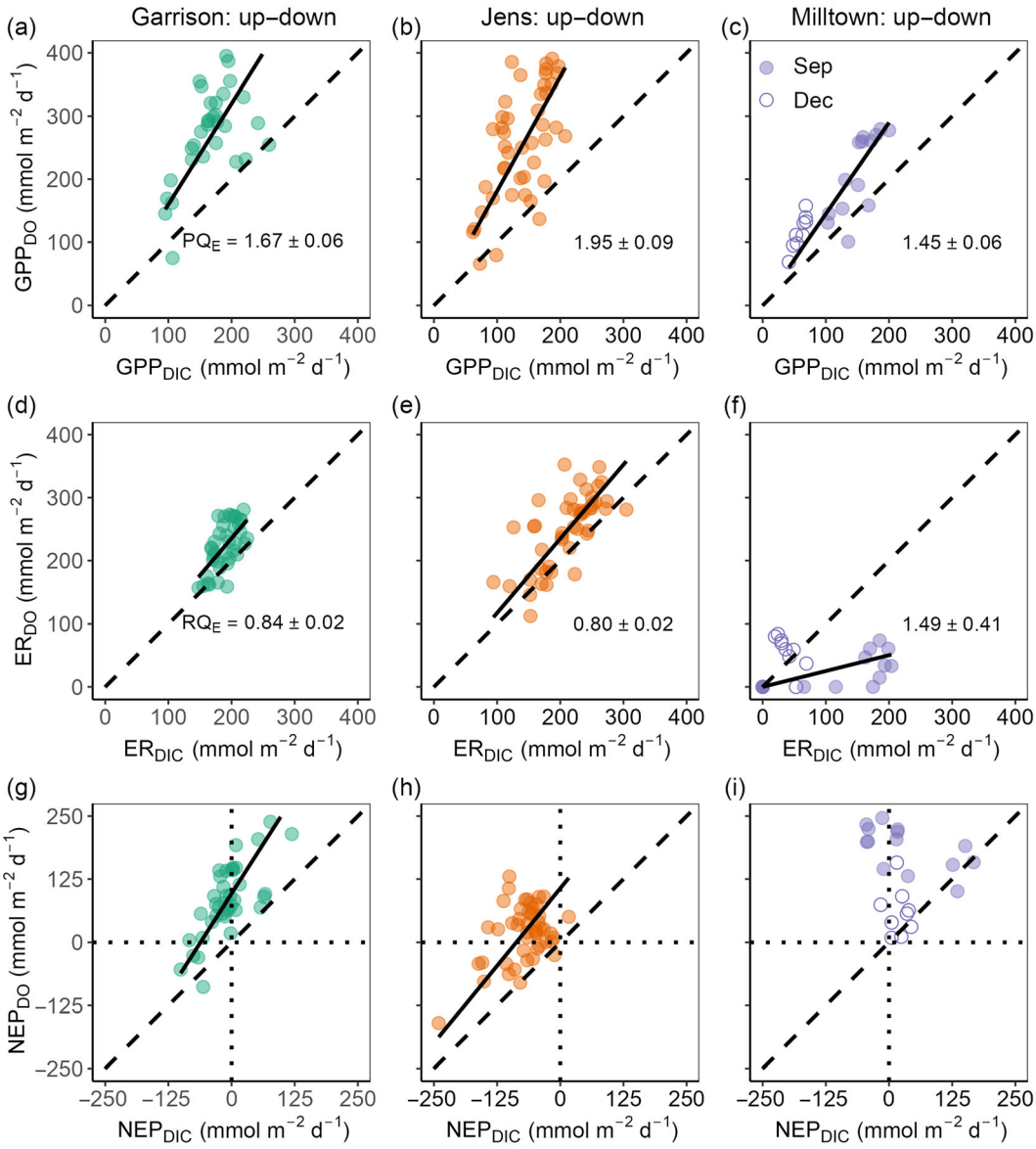

Fig. 6. Comparison of metabolism parameters estimated using DO (*y*-axis) and DIC (*x*-axis) data. Slopes of regressions between GPP_{DIC} (*x*-axis) and GPP_{DO} (*y*-axis) represent ecosystem-level photosynthetic quotient (PQ_E), while the inverse of slopes between ER_{DIC} (*x*-axis) and ER_{DO} (*y*-axis) represent respiration quotient (RQ_E). Intercepts of the regressions for PQ_E and RQ_E were fixed at 0 mmol m^{-2} d^{-1}. NEP_{DIC} was compared to NEP_{DO} by RMA regression. All metabolism estimates are from two-station models (up–down). Top panel: (**a–c**) for PQ_E at Garrison, Jens, and Milltown. September and December data at Milltown are indicated by filled and open circles, respectively. $PQ_E > 1$ with $GPP_{DO} > GPP_{DIC}$. Middle panel: (**d–f**) for RQ_E as the inverse of regression slopes. $RQ_E < 1$ with $ER_{DO} < ER_{DIC}$ except for Milltown. Bottom panel: $NEP_{DIC} < NEP_{DO}$ by an average of 100 mmol m^{-2} d^{-1}. RMA showed $y = (1.57 \pm 0.18)x + (96 \pm 9)$ for Garrison (**g**) and $y = (1.23 \pm 0.17)x + (109 \pm 15)$ for Jens (**h**), and no relationship for Milltown (**i**). Dotted lines indicate zero lines. PQ_E and RQ_E deviated from conventional values of one in alignment with the difference between NEP_{DIC} and NEP_{DO}. DIC, dissolved inorganic carbon; DO, dissolved oxygen; ER, ecosystem respiration; GPP, gross primary production; NEP, net ecosystem production; RMA, reduced major axis.

Jens, and Milltown, respectively (Fig. 6d–f), meaning $ER_{DO} > ER_{DIC}$ except for Milltown (Eq. 5). Individual RQ_E at Garrison and Jens were mostly < 1, and there were a few outlier estimates (> 3) at Milltown (Supporting Information Fig. S9b), likely due to inaccurate estimates from the weak diel cycles of DO and pCO_2 (Supporting Information Fig. S3). NEP_{DO} indicated mostly autotrophic conditions and NEP_{DIC} indicated net heterotrophy in accordance with $PQ_E > 1$ and $RQ_E < 1$ (Fig. 6g–i). At Garrison and Jens, regressions between NEP_{DIC} and NEP_{DO} yielded slopes of 1.57 ± 0.18 and 1.23 ± 0.17, and intercepts of 96 ± 9 and 109 ± 15 mmol m^{-2} d^{-1}, respectively. At Milltown, NEP_{DIC}

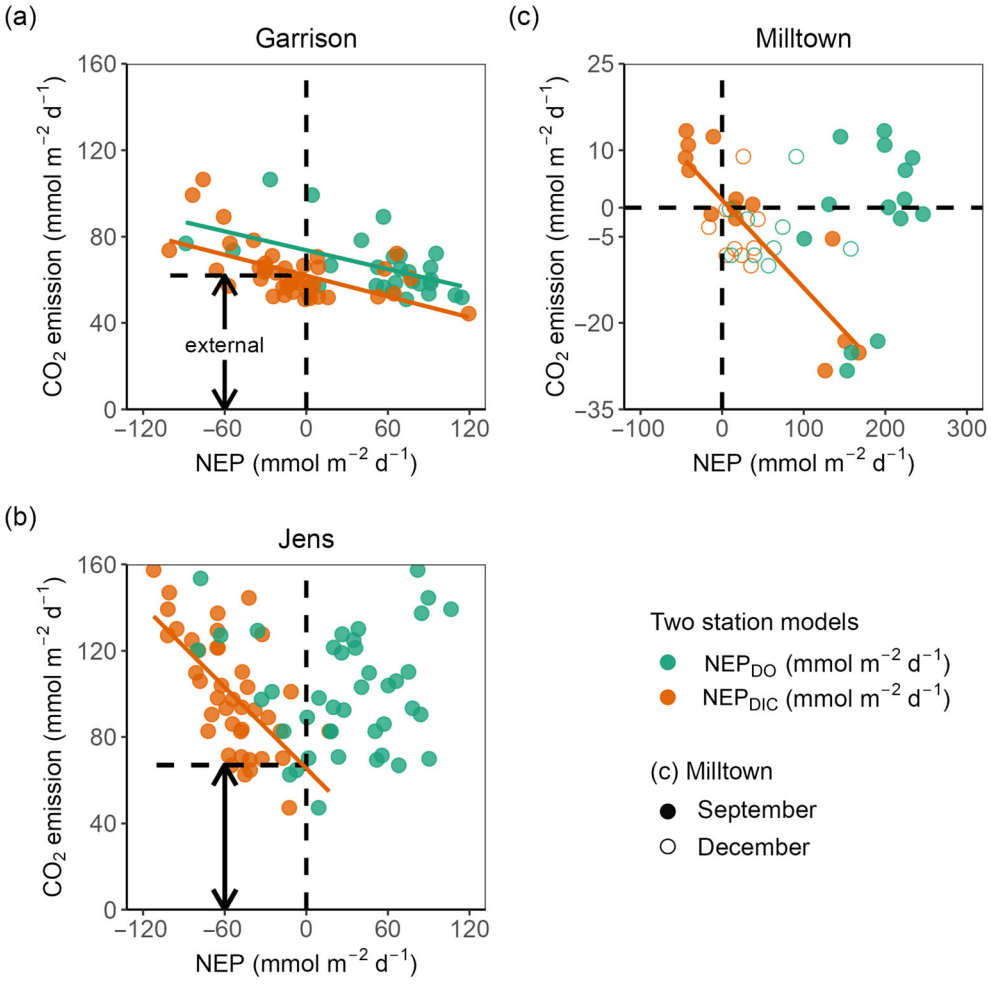

Fig. 7. Examination of the relationship between daily CO_2 emission and metabolism. Metabolism is NEP_{DO} in green and NEP_{DIC} in orange, which were compared to CO_2 emissions in regressions. The autotrophic NEP_{DO} and heterotrophic NEP_{DIC} provided contrasting views into the role of metabolism in producing CO_2. All metabolism estimates are from two-station models. (**a**) Garrison. (**b**) Jens. (**c**) Milltown in September (filled circles) and December (open circles). The two seasonal deployments at Milltown were grouped for regressions. Dashed lines represent zero NEP or zero CO_2 emission in (**c**). For Garrison and Jens, the regression intercepts suggested an external source of CO_2 from upstream of the reach. Regressions between NEP_{DO} and CO_2 emissions are not shown in Jens and Milltown (**b**,**c**) due to the weak relationship. DIC, dissolved inorganic carbon; DO, dissolved oxygen; NEP, net ecosystem production; RMA, reduced major axis

and NEP_{DO} had weak $(R^2 = 0.03)$ or nonsensical (negative) regressions (Fig. 6i) caused by the difficulty in inferring ER.

Linking metabolism to CO_2 emissions

Relations between daily CO_2 emission and NEP depended on how we measured NEP, with NEP_{DO} and NEP_{DIC} pointing to contrasting roles of metabolism (Fig. 7). NEP should strongly covary with CO_2 emissions. Comparing both NEP_{DO} and NEP_{DIC} with CO_2 emissions showed that the more negative NEP_{DIC} produced greater CO_2 emissions, but $NEP_{DO} > 0$ did not follow CO_2 emissions except for Garrison. The slopes of the regression model between CO_2 emissions and NEP_{DIC} were -0.16 ± 0.04 $(R^2 = 0.32)$ at Garrison, -0.64 ± 0.08 $(R^2 = 0.56)$ at Jens, and -0.15 ± 0.02 $(R^2 = 0.69)$ at Milltown. Jens demonstrated the largest changes in emissions with changes in NEP_{DIC}, and thus had the largest influence from in-stream CO_2 production. Based on the intercepts of the regression model, CO_2 emissions due to external sources were similar at Garrison and Jens (62 ± 2 and 67 ± 7 mmol m^{-2} d^{-1}). Milltown had the lowest intercept of 1.3 ± 1.5 mmol m^{-2} d^{-1}, demonstrating minimal external influence. Relative to the baseline of external CO_2, NEP_{DIC} as much as doubled CO_2 emissions at Garrison and Jens (Fig. 7a, b). At Milltown, NEP_{DIC} completely explained CO_2 emissions (or CO_2 influx) from the atmosphere (± 100%) (Fig. 7c). Nevertheless, the regression model for NEP_{DO} greatly changed interpretations of CO_2 sources at Garrison, and did not provide quantitative information at Jens and Milltown.

Discussion

Metabolism estimates differed when using a new DIC model compared with results by conventional methods using DO. The two-station approach may be needed for comparing DO and DIC metabolism. The two-station approach deviated from the single-station approach for DIC but less strongly for DO at Garrison (Fig. 5), which could be explained by the different time scales for DO and CO_2 to equilibrate with the atmosphere (Fig. 1). With the two-station approach, the divergent DO and DIC metabolism estimates demonstrate the potential for variation in stoichiometry (PQ_E and RQ_E) to complicate our understanding of oxygen and carbon processing in rivers (Fig. 6). Our assessment of DIC metabolism adds a new perspective on in-stream metabolic processes, terrestrial inputs, and CO_2 emissions (Fig. 7). Understanding the differences between the DO and DIC metabolism will increase our understanding of how in-stream processes control DIC cycling.

The difference in upstream influence between DO and DIC

Because of the carbonate buffering in rivers with circumneutral pH, CO_2 in the DIC pool takes longer to erase the air–water gradient than DO (Stets et al. 2017), which could compromise its use in single-station metabolism models. The entire DIC pool comprises CO_2 (including carbonic acid), HCO_3^-, and CO_3^{2-} (Fig. 1). In alkaline waters, HCO_3^- is much more abundant than the other two. For example, HCO_3^- is 80% of DIC at pH = 7 and 97% at pH = 8; thus, much of DIC travels longitudinally in the form of HCO_3^-, which generates a long-term effect on CO_2 dynamics via the equilibration between HCO_3^- and CO_2 (Supporting Information Eq. S3). Consequently, the influencing reach may be considerably longer than that for DO. Stets et al. (2017) simulated the time periods for CO_2 equilibration with the atmosphere at $A_T = 1000$ and $2500\,\mu mol\,L^{-1}$, both of which are clearly longer than that for DO with a longer equilibration period for the high A_T (*see* Fig. 5a,c therein). The long memory of past DIC concentrations for a heterogeneous reach may easily cause uncertainty in linking single-station metabolism estimates to a specific reach. The same notion was proposed by Hensley and Cohen (2016) to contrast dynamics of nitrate and DO. At Garrison, the discrepancy between single- and two-station DIC models (Fig. 5a,b; Supporting Information Table S7; Fig. S8) is likely caused by the upstream heterogeneity introduced by groundwater and waste water effluent. By contrast, the strong correspondence between single- and two-station models at Jens (Fig. 5c,d) reflects a greater degree of homogeneity within this study reach. The claim is supported by electrical conductivity signals, which were more correlated between upstream and downstream sites (Supporting Information 11; Fig. S10) and had more clear periodicity (Supporting Information Fig. S11) at Jens than at Garrison. More uniform conductivity signals between upstream and downstream sites indicate hydrological (e.g., evapotranspiration) and biological (e.g., CO_2 uptake) processes are more homogeneous (Vogt et al. 2010; Schmidt et al. 2012). The two-station model may generate more reliable estimates of DIC metabolism because rivers are not likely to be homogeneous at the scale of the river length necessary to remove most of the upstream CO_2 influence. For low A_T rivers, the single- and two-station DIC models may have a higher chance of providing similar metabolism estimates. An analytical solution of how the influencing reach length changes over a sequence of A_T or pH should be the subject of a future study.

Implementing two-station studies of metabolism requires consideration of reach length, complete mixing of representative river water at monitoring stations, and quality assurance of data to avoid compounding error. First, τ is a critical parameter for the two-station model and is controlled by sensor placement which is often dictated by accessibility. At Garrison, for example, we observed the increased regression uncertainty when comparing metabolism estimates between up–down ($\tau = 180$ min) and up–mid ($\tau = 75$ min) sub-reaches (Supporting Information 8; Table S6; Fig. S7). Second, two-station models require more data collection (two sensors instead of one) and accurate sensor calibration. Any systematic offset in sensor data would likely result in error in the estimate of ER (Holtgrieve et al. 2010; Schechner et al. 2021), particularly for pCO_2 close to saturation values like in Milltown (Supporting Information Fig. S3). Collecting samples for quality control of DO and pCO_2 and co-locating sensors in situ prior to two-station deployment are critical to ensure that measurement errors contribute as little as possible to errors in metabolism estimates.

Metabolic stoichiometry of DIC and DO processing

PQ_E and RQ_E clearly deviated from biochemical PQ and RQ. The differences between NEP_{DO} and NEP_{DIC} varied around 100 mmol m^{-2} d^{-1} (Fig. 6g–i), emphasizing the large uncertainty of using biochemical PQ and RQ for DO metabolism. Note the uncertainty of K_{600} cannot cause the NEP discrepancy given the limited sensitivity of two-station NEP to K_{600} (Fig. 3c,d; Supporting Information 6), and because we fixed the same K_{600} for both DO and DIC two-station models. PQ_E and RQ_E could encompass a wider range than conventional PQ and RQ. PQ and RQ are directly linked to the elemental composition of organic products or substrates in natural aquatic ecosystems (Laws 1991), and are conceptually analogous to the Redfield ratio of the planktonic communities in marine ecosystems (Redfield 1958). PQ_E and RQ_E not only incorporate variations in PQ and RQ, but also processes other than aerobic metabolism that drive a variable stoichiometric relationship of DO and DIC. Trentman et al. (2023) found a range of $PQ_E = 0.1 - 4.2$ in the literature, and Berggren et al. (2012) measured RQ_E of 0.25–2.26 (1.2 ± 0.45 as mean ± SD) by incubation in a myriad of lakes and ponds. Biochemical PQ appeared not to be useful for the Clark Fork River: Trentman

et al. (2023) predicted biochemical PQ to range from 0.5 to 0.9 in the same sites on the Clark Fork, which is far lower than the PQ_E estimated here. Noteworthy, all PQ_E reported here are all within the uncertainty range of 1.6 ± 0.5 by chamber measurements in the same river (Trentman et al. 2023).

CO_2 production by physical and biological processes other than aerobic respiration could explain the divergent finding of DIC heterotrophy and DO autotrophy in the Upper Clark Fork River. These processes would increase observed RQ_E, breaking the reciprocal relationship with PQ_E (Eq. 5). Denitrification, for example, is anaerobic respiration that produces CO_2 without consuming DO (Burgin and Loecke 2023). Madinger and Hall (2019) measured the molar ratio of denitrification to DO respiration around 1.1% in mountain headwater streams, but the ratio can be higher in high nitrate rivers (Reisinger et al. 2016). The Upper Clark Fork River is productive relative to other rivers (Savoy et al. 2019) with high incident light and large spatial gradients of nitrate (Valett et al. 2022), and may thus support high rates of denitrification. Photo-oxidation of organic matter (Rocher-Ros et al. 2021) can increase DIC and consume DO, but its potential influence on RQ_E is less clear because the molar ratio of CO_2 and DO due to photochemical processes is pathway-dependent (Ward and Cory 2020). In addition, calcite formation in the vicinity of photosynthetic cells (Tobias and Böhlke 2011) can occur under well-lit, high pH and A_T conditions. In the Clark Fork River, calcite saturation states ranged from 5 to 30 (Shangguan et al. 2021), and therefore calcite precipitation possibly occurred. We ignored this process by assuming a constant A_T. Yet, our simulation results suggest that calcite precipitation could lower NEP_{DIC} by $< 12\ \text{mmol m}^{-2}\ \text{d}^{-1}$ under scenarios of variable A_T (Supporting Information 5; Table S3). Finally, although we selected sites with minimal change in flow from upstream to downstream, small volumes of groundwater would be difficult to detect between the two stations. Groundwater inputs could increase river CO_2 but decrease DO by a smaller non-stoichiometric magnitude. Therefore, groundwater potentially causes different systematic errors in both ER_{DIC} and ER_{DO} (Hall and Tank 2005).

Different photosynthetic pathways might explain $GPP_{DIC} < GPP_{DO}$, and therefore $NEP_{DIC} < NEP_{DO}$. One model assumption is that DIC uptake via photosynthesis does not change A_T, that is, the charge balance. If algae take up CO_2, then we expect negligible change to A_T. On the other hand, if they use carbonic anhydrase to convert HCO_3^- to CO_2, then the effect on A_T will depend on the specifics of that process. Algae possess a diversity of ways to concentrate inorganic carbon using carbonic anhydrase (Maberly and Gontero 2017), including direct uptake of $NaHCO_3$, which would lower A_T. Evidence for ecosystem-level effects of this process comes from Aho et al. (2021) who found high rates of photosynthesis at low CO_2 concentrations; such a pattern is consistent with direct HCO_3^- uptake and if occurring in the Clark Fork River, could explain why $GPP_{DIC} < GPP_{DO}$. However, in the Clark Fork River, the minimum CO_2 concentrations ($K_{H,t} \cdot P_{CO_2,t}$ in Eq. 2) were $8\ \mu\text{mol L}^{-1}$ and CO_2 depletion was not observed as in Aho et al. (2021).

Despite $NEP_{DO} > NEP_{DIC}$, processes that decrease NEP_{DO} by consuming or losing DO may also occur. The resulting flux of DO must be smaller than flux of CO_2 production by processes like denitrification. DO has large diel swings and is frequently above 100% saturation in the river (Supporting Information Figs. S2, S3b1,b2), creating favorable conditions for photorespiration. Generally, photorespiration decreases PQ_E by consuming 3 mol of DO and producing only 1 mol of CO_2 (Stewart 1974). Similarly, nitrification can consume DO while fixing only a small amount of CO_2; this flux can be high in high N rivers (Pathak et al. 2022). Finally, ebullition could also decrease PQ_E when oxygen is released into the atmosphere via bubbles. Undissolved gas bubbles produced by primary producers are not measured by sensors and therefore not modeled into GPP_{DO}. These processes potentially contribute to the observed difference between NEP_{DO} and NEP_{DIC} and the large range of PQ_E and RQ_E. Taken together, the myriad of processes that control DIC and DO outside of the cellular reactions of photosynthesis and respiration complicate our ability to predict or understand the causes in variation in PQ_E and RQ_E.

NEP and CO_2 emissions

Although assessments of relationships between NEP and CO_2 emissions were sensitive to whether metabolism was estimated from DO or DIC, large variations of NEP and CO_2 emissions suggest the substantial contribution of metabolism in the Clark Fork River. Other studies have also demonstrated that the contributions of in-stream metabolic processes can exceed those of groundwater inputs to supply CO_2 emissions (Bernal et al. 2022; Carter et al. 2022). For our study sites, the slopes of regression between NEP_{DIC} and CO_2 emissions < 1 suggests that CO_2 emissions were constrained by k_{CO_2} (Rocher-Ros et al. 2019), supported by the low K_{600} of $12\ \text{d}^{-1}$ from DO models (Supporting Information Fig. S5). Every mole of in-stream CO_2 production was only partially emitted over the reach. For the same reason, the external sources at Garrison and Jens (Fig. 7a,b) include parts of in-stream CO_2 production imported from upstream and groundwater-delivered DIC. The low CO_2 emissions at the downstream Milltown reach were almost completely driven by NEP_{DIC} with negligible external sources (Fig. 7c), which is in agreement with low Radon-222 concentration near the reach (Horne 2017). Consequently, NEP was greater than CO_2 emissions (Fig. 7c), similar to findings at a tropical stream (Solano et al. 2023).

Conclusion

In this work, we showed that the DIC metabolism modeled from pCO_2 and A_T differed from DO metabolism. The DIC model enabled us to evaluate the best strategies for estimating metabolism from pCO_2 data. A two-station approach is

essential for estimating DIC metabolism when pH is high enough that HCO_3^- comprises a substantial fraction of DIC. Although the single-station DIC model gave similar metabolism results in some reaches, it is not possible to readily predict homogeneity for a longer influencing reach and therefore single-station DIC results will be questionable. Yet, in acidic rivers, the upstream influencing reach should be greatly shortened which, we suggest, should be evaluated in future work before using the single-station DIC model. It is necessary to account for carbonate buffering for pCO_2 at each time step in order to correctly implement the DIC two-station model. High quality pCO_2 data reduce systematic errors and noise in metabolism results. Next, based on DIC modeling methods in conjunction with commonly used DO, our results show NEP_{DIC} was lower than NEP_{DO} by an average of 100 mmol m^{-2} d^{-1} in the Upper Clark Fork River. The difference between NEP_{DIC} and NEP_{DO} was reflected by $PQ_E > 1$ and $RQ_E < 1$, confounding our interpretations of how in-stream processes contribute to CO_2 emissions. The linkage between diel cycles of DIC and DO is likely driven by multiple physical and biological processes as opposed to aerobic metabolism only, some of which may be unknown or unmeasured. Due to this complexity, it is difficult to predict PQ_E by assuming certain processes exist in rivers (Trentman et al. 2023); direct estimates are required that involve more data collection and modeling.

The variability in PQ_E and RQ_E becomes a source of uncertainty in studies of metabolism and carbon cycling using long-term DO sensor data. DO time series on annual scales have been more commonly available (e.g., Bernhardt et al. 2022) while CO_2 or DIC data are relatively limited. It is encouraging, however, that PQ_E estimates in the same river were similar (Fig. 6a–c), possibly indicating a commonality of underlying mechanisms for their variability. Eventually, more information regarding PQ_E and RQ_E may reduce the uncertainty of using DO metabolism and more accurately constrain the global contributions of in-stream processes to carbon cycling.

Data availability statement

The data and codes that support the findings of this study can be accessed in the Environmental Data Initiative repository (https://doi.org/10.6073/pasta/7b5d1fe9a3d17847a9cf5012da2a3456).

References

Aho, K. S., J. D. Hosen, L. A. Logozzo, W. R. McGillis, and P. A. Raymond. 2021. Highest rates of gross primary productivity maintained despite CO_2 depletion in a temperate river network. Limnol. Oceanogr. Lett. **6**: 200–206. doi:10.1002/lol2.10195

Andrews, A., and others. 2020. Continuous measurements of CO_2, CO, CH_4 on tall towers starting in 1992. NOAA Earth System Research Laboratory, Global Monitoring Division. doi:10.7289/V57W69F2

Appling, A. P., R. O. Hall, C. B. Yackulic, and M. Arroita. 2018. Overcoming equifinality: Leveraging long time series for stream metabolism estimation. J. Geophys. Res. Biogeosci. **123**: 624–645. doi:10.1002/2017JG004140

Battin, T. J., and others. 2023. River ecosystem metabolism and carbon biogeochemistry in a changing world. Nature **613**: 449–459. doi:10.1038/s41586-022-05500-8

Berggren, M., J.-F. Lapierre, and P. A. Del Giorgio. 2012. Magnitude and regulation of bacterioplankton respiratory quotient across freshwater environmental gradients. ISME J. **6**: 984–993. doi:10.1038/ismej.2011.157

Bernal, S., M. J. Cohen, J. L. Ledesma, L. Kirk, E. Martí, and A. Lupon. 2022. Stream metabolism sources a large fraction of carbon dioxide to the atmosphere in two hydrologically contrasting headwater streams. Limnol. Oceanogr. **67**: 2621–2634. doi:10.1002/lno.12226

Bernhardt, E. S., and others. 2022. Light and flow regimes regulate the metabolism of rivers. Proc. Natl. Acad. Sci. USA **119**: e2121976119. doi:10.1073/pnas.2121976119

Burgin, A., and T. Loecke. 2023. The biogeochemical redox paradox: How can we make a foundational concept more predictive of biogeochemical state changes? Biogeochemistry **164**: 349–370. doi:10.1007/s10533-023-01036-9

Butman, D., and P. A. Raymond. 2011. Significant efflux of carbon dioxide from streams and rivers in the United States. Nat. Geosci. **4**: 839–842. doi:10.1038/NGEO1294

Butman, D., S. Stackpoole, E. Stets, C. P. McDonald, D. W. Clow, and R. G. Striegl. 2016. Aquatic carbon cycling in the conterminous United States and implications for terrestrial carbon accounting. Proc. Natl. Acad. Sci. USA **113**: 58–63. doi:10.1073/pnas.1512651112

Carpenter, J. H. 1965. The Chesapeake Bay institute technique for the Winkler dissolved oxygen method. Limnol. Oceanogr. **10**: 141–143. doi:10.4319/lo.1965.10.1.0141

Carter, A. M., A. G. DelVecchia, and E. S. Bernhardt. 2022. Patterns and drivers of dissolved gas concentrations and fluxes along a low gradient stream. J. Geophys. Res. Biogeosci. **127**: e2022JG007048. doi:10.1029/2022JG007048

Carvalho, M. C. 2014. Net seaweed photosynthesis measured from changes in natural stable carbon isotope ratios in incubation water. Phycologia **53**: 488–492. doi:10.2216/14-052.1

Cole, J. J., and others. 2007. Plumbing the global carbon cycle: Integrating inland waters into the terrestrial carbon budget. Ecosystems **10**: 172–185. doi:10.1007/s10021-006-9013-8

Crawford, J. T., N. R. Lottig, E. H. Stanley, J. F. Walker, P. C. Hanson, J. C. Finlay, and R. G. Striegl. 2014. CO_2 and CH_4 emissions from streams in a lake-rich landscape: Patterns, controls, and regional significance. Global Biogeochem. Cycles **28**: 197–210.

DeGrandpre, M., T. Hammar, S. Smith, and F. Sayles. 1995. In situ measurements of seawater pCO_2. Limnol. Oceanogr. **40**: 969–975.

Demars, B. O., J. Thompson, and J. R. Manson. 2015. Stream metabolism and the open diel oxygen method: Principles, practice, and perspectives. Limnol. Oceanogr. Methods **13**: 356–374. doi:10.1002/lom3.10030

Dickson, A. G., C. L. Sabine, and J. R. Christian. 2007. Guide to best practices for ocean CO_2 measurements. North Pacific Marine Science Organization.

Dodds, W., V. Smith, and B. Zander. 1997. Developing nutrient targets to control benthic chlorophyll levels in streams: A case study of the Clark Fork River. Water Res. **31**: 1738–1750. doi:10.1016/S0043-1354(96)00389-2

Drake, T. W., P. A. Raymond, and R. G. Spencer. 2018. Terrestrial carbon inputs to inland waters: A current synthesis of estimates and uncertainty. Limnol. Oceanogr. Lett. **3**: 132–142. doi:10.1002/lol2.10055

Garcia, H. E., and L. I. Gordon. 1992. Oxygen solubility in seawater: Better fitting equations. Limnol. Oceanogr. **37**: 1307–1312. doi:10.4319/lo.1992.37.6.1307

Gómez-Gener, L., and others. 2016. Low contribution of internal metabolism to carbon dioxide emissions along lotic and lentic environments of a Mediterranean fluvial network. J. Geophys. Res. Biogeosci. **121**: 3030–3044. doi:10.1002/2016JG003549

Grace, M. R., D. P. Giling, S. Hladyz, V. Caron, R. M. Thompson, and R. Mac Nally. 2015. Fast processing of diel oxygen curves: Estimating stream metabolism with base (BAyesian Single-station Estimation). Limnol. Oceanogr. Methods **13**: 103–114. doi:10.1002/lom3.10011

Hall, R. O., and J. L. Tank. 2005. Correcting whole-stream estimates of metabolism for groundwater input. Limnol. Oceanogr. Methods **3**: 222–229. doi:10.4319/lom.2005.3.222

Hall, R. O., J. L. Tank, M. A. Baker, E. J. Rosi-Marshall, and E. R. Hotchkiss. 2016. Metabolism, gas exchange, and carbon spiraling in rivers. Ecosystems **19**: 73–86. doi:10.1007/s10021-015-9918-1

Hall, R. O., and E. R. Hotchkiss. 2017. Stream metabolism, p. 219–233. *In* Methods in stream ecology. Elsevier.

Hensley, R. T., and M. J. Cohen. 2016. On the emergence of diel solute signals in flowing waters. Water Resour. Res. **52**: 759–772. doi:10.1002/2015WR017895

Holtgrieve, G. W., D. E. Schindler, T. A. Branch, and Z. T. A'mar. 2010. Simultaneous quantification of aquatic ecosystem metabolism and reaeration using a Bayesian statistical model of oxygen dynamics. Limnol. Oceanogr. **55**: 1047–1063. doi:10.4319/lo.2010.55.3.1047

Horne, M. 2017. Detecting regional groundwater discharge to the Clark Fork River. Master's thesis, Univ. of Montana.

Hotchkiss, E. R., and R. O. Hall. 2014. High rates of daytime respiration in three streams: Use of $\delta^{18}O_{O_2}$ and O_2 to model diel ecosystem metabolism. Limnol. Oceanogr. **59**: 798–810. doi:10.4319/lo.2014.59.3.0798

Hotchkiss, E. R., R. Hall, R. Sponseller, D. Butman, J. Klaminder, H. Laudon, M. Rosvall, and J. Karlsson. 2015. Sources of and processes controlling CO_2 emissions change with the size of streams and rivers. Nat. Geosci. **8**: 696–699. doi:10.1038/NGEO2507

Howard, E. M., I. Forbrich, A. E. Giblin, D. E. Lott III, K. L. Cahill, and R. H. Stanley. 2018. Using noble gases to compare parameterizations of air–water gas exchange and to constrain oxygen losses by ebullition in a shallow aquatic environment. J. Geophys. Res. Biogeosci. **123**: 2711–2726. doi:10.1029/2018JG004441

Jähne, B., K. O. Münnich, R. Bösinger, A. Dutzi, W. Huber, and P. Libner. 1987. On the parameters influencing air–water gas exchange. J. Geophys. Res. Oceans **92**: 1937–1949. doi:10.1029/JC092iC02p01937

Kelly, M. G., N. Thyssen, and B. Moeslund. 1983. Light and the annual variation of oxygen-and carbon-based measurements of productivity in a macrophyte-dominated river. Limnol. Oceanogr. **28**: 503–515.

Lai, C.-Z., and others. 2016. Spectrophotometric measurement of freshwater pH with purified meta-cresol purple and phenol red. Limnol. Oceanogr. Methods **14**: 864–873. doi:10.1002/lom3.10137

Langdon, C. 1984. Dissolved oxygen monitoring system using a pulsed electrode: Design, performance, and evoluation. Deep-Sea Res. I Oceanogr. Res. Pap. **31**: 1357–1367. doi:10.1016/0198-0149(84)90006-2

Lauerwald, R., G. G. Laruelle, J. Hartmann, P. Ciais, and P. A. Regnier. 2015. Spatial patterns in CO_2 evasion from the global river network. Global Biogeochem. Cycles **29**: 534–554. doi:10.1002/2014GB004941

Laws, E. A. 1991. Photosynthetic quotients, new production and net community production in the open ocean. Deep-Sea Res. I Oceanogr. Res. Pap. **38**: 143–167. doi:10.1016/0198-0149(91)90059-O

Lynch, J. K., C. M. Beatty, M. P. Seidel, L. J. Jungst, and M. D. DeGrandpre. 2010. Controls of riverine CO_2 over an annual cycle determined using direct, high temporal resolution pCO_2 measurements. J. Geophys. Res. Biogeosci. **115**: G03016.

Maberly, S. C., and B. Gontero. 2017. Ecological imperatives for aquatic CO_2-concentrating mechanisms. J. Exp. Bot. **68**: 3797–3814. doi:10.1093/jxb/erx201

Madinger, H. L., and R. O. Hall. 2019. Linking denitrification with ecosystem respiration in mountain streams. Limnol. Oceanogr. Lett. **4**: 145–154. doi:10.1002/lol2.10111

Moore, J. N., and H. W. Langner. 2012. Can a river heal itself? Natural attenuation of metal contamination in river sediment. Environ. Sci. Technol. **46**: 2616–2623.

Odum, H. T. 1956. Primary production in flowing waters 1. Limnol. Oceanogr. **1**: 102–117.

Pathak, D., and others. 2022. High-resolution water-quality and ecosystem-metabolism modeling in lowland rivers. Limnol. Oceanogr. **67**: 1313–1327. doi:10.1002/lno.12079

Payn, R. A., R. Hall, T. A. Kennedy, G. C. Poole, and L. A. Marshall. 2017. A coupled metabolic-hydraulic model and calibration scheme for estimating whole-river metabolism during dynamic flow conditions. Limnol. Oceanogr. Methods **15**: 847–866.

Pennington, R., A. Argerich, and R. Haggerty. 2018. Measurement of gas-exchange rate in streams by the oxygen–carbon method. Freshw. Sci. **37**: 222–237.

R Core Team. 2018. R: A language and environment for statistical computing. R Foundation for Statistical Computing.

Raymond, P. A., and others. 2012. Scaling the gas transfer velocity and hydraulic geometry in streams and small rivers. Limnol. Oceanogr. Fluids Environ. **2**: 41–53. doi:10.1215/21573689-1597669

Raymond, P. A., and others. 2013. Global carbon dioxide emissions from inland waters. Nature **503**: 355–359.

Redfield, A. C. 1958. The biological control of chemical factors in the environment. Am. Sci. **46**: 205–221.

Reichert, P., U. Uehlinger, and V. Acuña. 2009. Estimating stream metabolism from oxygen concentrations: Effect of spatial heterogeneity. J. Geophys. Res. Biogeosci. **114**: G03016. doi:10.1029/2008JG000917

Reisinger, A. J., J. L. Tank, T. J. Hoellein, and R. O. Hall Jr. 2016. Sediment, water column, and open-channel denitrification in rivers measured using membrane-inlet mass spectrometry. J. Geophys. Res. Biogeosci. **121**: 1258–1274. doi:10.1002/2015JG003261

Reynolds, J. C. 2001. Distributed in situ gas measurements for the analysis and modeling of biogeochemical changes in the Clark Fork River. Master's thesis, Univ. of Montana.

Rocher-Ros, G., R. A. Sponseller, W. Lidberg, C.-M. Mörth, and R. Giesler. 2019. Landscape process domains drive patterns of CO_2 evasion from river networks. Limnol. Oceanogr. Lett. **4**: 87–95. doi:10.1002/lol2.10108

Rocher-Ros, G., R. A. Sponseller, A.-K. Bergström, M. Myrstener, and R. Giesler. 2020. Stream metabolism controls diel patterns and evasion of CO_2 in Arctic streams. Global Change Biol. **26**: 1400–1413. doi:10.1111/gcb.14895

Rocher-Ros, G., T. K. Harms, R. A. Sponseller, M. Väisänen, C.-M. Mörth, and R. Giesler. 2021. Metabolism overrides photo-oxidation in CO_2 dynamics of Arctic permafrost streams. Limnol. Oceanogr. **66**: S169–S181. doi:10.1002/lno.11564

Savoy, P., A. P. Appling, J. B. Heffernan, E. G. Stets, J. S. Read, J. W. Harvey, and E. S. Bernhardt. 2019. Metabolic rhythms in flowing waters: An approach for classifying river productivity regimes. Limnol. Oceanogr. **64**: 1835–1851. doi:10.1002/lno.11154

Schechner, A. E., W. K. Dodds, F. Tromboni, S. Chandra, and A. Maasri. 2021. How do methodological choices influence estimation of river metabolism? Limnol. Oceanogr. Methods **19**: 659–672. doi:10.1002/lom3.10451

Schmidt, C., A. Musolff, N. Trauth, M. Vieweg, and J. Fleckenstein. 2012. Transient analysis of fluctuations of electrical conductivity as tracer in the stream bed. Hydrol. Earth Syst. Sci. **16**: 3689–3697. doi:10.5194/hess-16-3689-2012

Shangguan, Q., C.-Z. Lai, C. M. Beatty, F. L. Young, R. S. Spaulding, and M. D. DeGrandpre. 2021. Autonomous in situ measurements of freshwater alkalinity. Limnol. Oceanogr. Methods **19**: 51–66. doi:10.1002/lom3.10404

Solano, V., C. Duvert, C. Birkel, D. T. Maher, E. A. García, and L. B. Hutley. 2023. Stream respiration exceeds CO_2 evasion in a low-energy, oligotrophic tropical stream. Limnol. Oceanogr. **68**: 1132–1146. doi:10.1002/lno.12334

Stets, E. G., R. G. Striegl, G. R. Aiken, D. O. Rosenberry, and T. C. Winter. 2009. Hydrologic support of carbon dioxide flux revealed by whole-lake carbon budgets. J. Geophys. Res. Biogeosci. **114**: G01008.

Stets, E. G., D. Butman, C. P. McDonald, S. M. Stackpoole, M. D. DeGrandpre, and R. G. Striegl. 2017. Carbonate buffering and metabolic controls on carbon dioxide in rivers. Global Biogeochem. Cycles **31**: 663–677. doi:10.1002/2016GB005578

Stewart, W. D. P. 1974. Algal physiology and biochemistry, v. **10**. Univ of California Press.

Suplee, M. W., V. Watson, W. K. Dodds, and C. Shirley. 2012. Response of algal biomass to large-scale nutrient controls in the Clark Fork River, Montana, United States. J. Am. Water Resour. Assoc. **48**: 1008–1021. doi:10.1111/j.1752-1688.2012.00666.x

Tobias, C., and J. K. Böhlke. 2011. Biological and geochemical controls on diel dissolved inorganic carbon cycling in a low-order agricultural stream: Implications for reach scales and beyond. Chem. Geol. **283**: 18–30. doi:10.1016/j.chemgeo.2010.12.012

Trentman, M. T., R. O. Hall, and H. M. Valett. 2023. Exploring the mismatch between the theory and application of photosynthetic quotients in aquatic ecosystems. Limnol. Oceanogr. Lett. **8**: 565–579. doi:10.1002/lol2.10326

Valett, H. M., M. Peipoch, and G. C. Poole. 2022. Nutrient processing domains: Spatial and temporal patterns of material retention in running waters. Freshw. Sci. **41**: 195–214. doi:10.1086/719991

Vogt, T., E. Hoehn, P. Schneider, A. Freund, M. Schirmer, and O. A. Cirpka. 2010. Fluctuations of electrical conductivity as a natural tracer for bank filtration in a losing stream. Adv. Water Resour. **33**: 1296–1308. doi:10.1016/j.advwatres.2010.02.007

Ward, C. P., and R. M. Cory. 2020. Assessing the prevalence, products, and pathways of dissolved organic matter partial photo-oxidation in Arctic surface waters. Environ. Sci. Process. Impacts **22**: 1214–1223. doi:10.1039/C9EM00504H

Warton, D. I., and others. 2012. smatr 3–An R package for estimation and inference about allometric lines. Methods Ecol. Evol. **3**: 257–259. doi:10.1111/j.2041-210X.2011.00153.x

Weiss, R. 1974. Carbon dioxide in water and seawater: The solubility of a non-ideal gas. Mar. Chem. **2**: 203–215. doi:10.1016/0304-4203(74)90015-2

Wolf, E., and R. Olson. 1974. Computer program used to estimate primary productivity from pH and carbon dioxide data employing the upstream–downstream method. Technical report. Battelle Pacific Northwest Labs.

Wright, J. C., and I. Mills. 1967. Productivity studies on the Madison River, Yellowstone National Park 1. Limnol. Oceanogr. **12**: 568–577. doi:10.4319/lo.1967.12.4.0568

Yard, M. D., G. E. Bennett, S. N. Mietz, L. G. Coggins Jr., L. E. Stevens, S. Hueftle, and D. W. Blinn. 2005. Influence of topographic complexity on solar insolation estimates for the Colorado River, Grand Canyon, AZ. Ecol. Model. **183**: 157–172. doi:10.1016/j.ecolmodel.2004.07.027

Young, F. L., Q. Shangguan, C. M. Beatty, M. D. Gilsdorf, and M. D. DeGrandpre. 2022. Comparison of spectrophotometric and electrochemical pH measurements for calculating freshwater pCO_2. Limnol. Oceanogr. Methods **20**: 514–529. doi:10.1002/lom3.10501

Acknowledgments

We thank Rafael Feijó de Lima for conducting the tracer release experiment at the Garrison reach. Cory Beatty contributed greatly to sensor preparations and deployments. Claire Utzman assisted with discrete sample collection. Alice Carter provided valuable discussions about *streamMetabolizer*. Many undergraduate and graduate researchers in the Upper Clark Fork River working group participated in the survey of river depth. Venice Bayrd provided guidance in preparing data products for Environmental Data Initiative. Jason Reynolds conducted the Milltown experiments as part of his Masters Thesis. We also thank the Associate Editor and two anonymous reviewers for comments on the draft. This research was supported by the US National Science Foundation grants DEB-1655197 (Long-term Research in Environmental Biology) and OIA-1757351 (Montana EPSCor).

Conflict of Interest

Michael D. DeGrandpre is a co-owner of Sunburst Sensors, LLC, the company that manufactures the SAMI sensor technologies.

Submitted 26 December 2023
Revised 19 April 2024
Accepted 04 August 2024

Associate editor: Ryan A. Sponseller